MIT Libraries | DSpace@MIT

MIT Open Access Articles

High-precision observation of nonvolatile quantum anomalous Hall effect

The MIT Faculty has made this article openly available. ***Please share*** how this access benefits you. Your story matters.

Citation: Chang, Cui-Zu, Weiwei Zhao, Duk Y. Kim, Haijun Zhang, Badih A. Assaf, Don Heiman, Shou-Cheng Zhang, Chaoxing Liu, Moses H. W. Chan, and Jagadeesh S. Moodera. "High-Precision Realization of Robust Quantum Anomalous Hall State in a Hard Ferromagnetic Topological Insulator." Nat Mater 14, no. 5 (March 2, 2015): 473–477.

As Published: http://dx.doi.org/10.1038/nmat4204

Publisher: Nature Publishing Group

Persistent URL: http://hdl.handle.net/1721.1/104335

Version: Author's final manuscript: final author's manuscript post peer review, without publisher's formatting or copy editing

Terms of Use: Article is made available in accordance with the publisher's policy and may be subject to US copyright law. Please refer to the publisher's site for terms of use.

Massachusetts Institute of Technology

High-precision observation of nonvolatile quantum anomalous Hall effect

Cui-Zu Chang,[1] Weiwei Zhao,[2] Duk Y. Kim,[2] Haijun Zhang,[3] Badih A. Assaf,[4] Don Heiman,[4] Shou-Cheng Zhang,[3] Chaoxing Liu,[2] Moses H. W. Chan,[2] and Jagadeesh S. Moodera[1,5]

[1]*Francis Bitter Magnet Lab, Massachusetts Institute of Technology, Cambridge, MA 02139, USA*

[2]*The Center for Nanoscale Science and Department of Physics, The Pennsylvania State University, University Park, PA 16802-6300, USA*

[3]*Department of Physics, Stanford University, Stanford, CA 94305-4045, USA*

[4]*Department of Physics, Northeastern University, Boston, MA 02115, USA*

[5]*Department of Physics, Massachusetts Institute of Technology, Cambridge, MA 02139, USA*

Corresponding authors: czchang@mit.edu(C. Z. C.); wzhao@phys.psu.edu (W. Z.) and moodera@mit.edu (J. S. M.)

Abstract

The discovery of the integer quantum Hall (QH) effect in 1980 led to the realization of a topological electronic state with dissipationless currents circulating in one direction along the edge of a two dimensional electron layer under a strong magnetic field.[1,2] The quantum anomalous Hall (QAH) effect shares a similar physical phenomenon as the QH effect, whereas its physical origin relies on the intrinsic spin-orbit coupling and ferromagnetism.[3-13] Since the QAH effect does not require an external field and the associated Landau levels, it is believed that this effect has unique potential for applications in electronic devices with low-power consumption.[3-16] Recently, the QAH effect has been experimentally observed in thin films of the ferromagnetic topological insulators (FMTI), Cr-doped $(Bi,Sb)_2Te_3$.[14] However, in this system, a large residual longitudinal resistance $0.098h/e^2$ (~2.53kΩ) remains, and thus the Hall conductance is only around $0.987e^2/h$ at zero magnetic field, hampering the precise realization of this dissipationless topological state. Here we report

the experimental observation of the QAH effect in V-doped $(Bi,Sb)_2Te_3$ films with the zero-field longitudinal resistance down to 0.00013±0.00007*h*/*e*^{2} (~3.35±1.76Ω), Hall conductance reaching 0.9998±0.0006*e*^{2}/*h* and the Hall angle becoming as high as 89.993±0.004° at *T*=25mK, thus realizing the anomalous Hall transport with negligible dissipation in the absence of any initial magnetic field. The advantage of this system comes from the fact that it is a hard ferromagnet with a large coercive field (H_c>1.0T) and a relative high Curie temperature. This realization of nonvolatile QAH state in hard FMTIs is a major step towards dissipationless electronic applications without external fields.

The quantum anomalous Hall (QAH) effect describes the dissipationless quantized Hall transport in ferromagnetic materials in the absence of external magnetic fields.[3-13] The realization of the QAH effect in realistic materials requires two conditions: ferromagnetic insulating materials and topologically non-trivial electronic band structures.[5,12,13] It has been proposed that these two conditions can be satisfied by introducing ferromagnetism into topological insulators (TIs).[12,13.] Ferromagnetism can be achieved by doping TIs with transition metal atoms, such as Cr, V and Mn.[17,18,19] Indeed, the QAH effect has been reported in Cr-doped $(Bi,Sb)_2Te_3$ system.[14,15,16] Among the various transition metal atoms, V-doped Sb_2Te_3 exhibits the most stable ferromagnetism with a high Curie temperature (T_C).[17,18] This fact motivated us to explore the QAH effect in V-doped TI thin films.

Epitaxial thin films with various concentrations of V-doped Sb_2Te_3 were prepared by coevaporation in a molecular beam epitaxy (MBE) system. Excellent ferromagnetic response was found for all samples, consistent with the early experiments.[17,18] To achieve the insulating phase, a small amount of Bi was added to tune the chemical potential (see Supplementary Information).[20,21] We note that T_C and H_c varies little with Bi doping, even in the rather insulating

samples around the p-n crossover region, which indicates that there is a truly insulating ferromagnetic state in V-doped Sb_2Te_3.[21] In order to realize accurate and continuous tuning of the Fermi energy and carrier density (n_{2D}), electric-field gating was also employed. The heat-treated $SrTiO_3(111)$ substrate with a large dielectric constant serves as an effective bottom gate dielectric. The magneto-transport was measured on two samples, denoted as S1 and S2, using the standard six-terminal Hall bar configuration. (see Methods and Supplementary Information).[14,21]

Our magneto-transport on a four quintuple-layers (QL) $(Bi_{0.29}Sb_{0.71})_{1.89}V_{0.11}Te_3$ film (sample S1) as shown in Fig. 1, exhibits nearly ideal QAH behavior. At the charge neutral point V_g^0, the Hall resistance (ρ_{yx}) at zero magnetic field (labeled as $\rho_{yx}(0)$) displays the quantized value of $1.00019\pm0.00069 h/e^2$ (25.8178 ± 0.0177kΩ), while the longitudinal resistance (ρ_{xx}) at zero magnetic field (labeled as $\rho_{xx}(0)$) is only $0.00013\pm0.00007 h/e^2$ (~3.35 ± 1.76Ω) measured at T=25mK,[22] shown in Figs 1b and 1c. The ratio $\rho_{yx}(0)/\rho_{xx}(0)$ corresponds to an anomalous Hall angle of 89.993±0.004º. The corresponding Hall conductance at zero magnetic field (labeled as $\sigma_{yx}(0)$) is up to $0.9998\pm0.0006 e^2/h$ and longitudinal conductance at zero magnetic field (labeled as $\sigma_{xx}(0)$) is down to $0.00013\pm0.00007 e^2/h$. For comparison, $\rho_{xx}(0)$, $\sigma_{yx}(0)$, $\sigma_{xx}(0)$ and the anomalous Hall angle in the Cr-doped system are $0.098 h/e^2$(~2.53kΩ), $0.987 e^2/h$, $0.096 e^2/h$ and 84.40º at T=30mK, respectively,[14] noticeably different from the expected values. The precise values of these quantities at zero-field were not reported systematically in ref. 15 and 16. Additional measurement about temperature and gate voltage dependence has also been performed, showing that the QAH behavior with an anomalous Hall angle of 84.40º (the largest Hall angle in Cr doped system) in V-doped system is seen up to ~130mK. (see Supplementary Information).

What we have found in V-doped system is clearly a more precise experimental confirmation of the ideal QAH effect than that in Cr-doped system. To understand the differences between these two materials, we carried out direct comparison of the two systems. Our studies showed three main differences. (1) Figure 2a shows the dependence of T_C for 6QL films of $Sb_{2-x}Cr_xTe_3$ and $Sb_{2-x}V_xTe_3$ as a function of the Cr or V doping concentration x. The T_C of a FM material can be determined from the Arrott plot (see Supplementary Information).[23] At the same concentration x, the T_C for V doping is twice value than that for Cr doping. Having a higher T_C with low x is in the right direction for enhancing the temperature to obtain QAH state.[24] (2) The Hall traces for x=0.13 films are shown in Fig. 2b. In both cases, the square-shaped loops indicate the long-range ferromagnetic order with out-of-plane magnetic anisotropy.[25] The coercive field H_c for the $Sb_{1.87}V_{0.13}Te_3$ film is ~1.3T at T=2K, an order of magnitude larger than that of $Sb_{1.87}Cr_{0.13}Te_3$ with H_c~0.1T.[14-16,21] The large H_c of V-doped Sb_2Te_3 is clearly advantageous for a nonvolatile FMTI system.[26,27] (3) Remarkably, the n_{2D} of 6QL $Sb_{1.87}V_{0.13}Te_3$ is ~ $2.5\times10^{13}cm^{-2}$, about one half of n_{2D} in $Sb_{1.87}Cr_{0.13}Te_3$ (n_{2D}~$4.9\times10^{13}cm^{-2}$). The low n_{2D} in the parent material is beneficial because it reduces the amount of Bi doping required to drive the system towards a charge neutral state.[20]

The main difference between these two materials lies in different magnetic moments and valence of V and Cr atoms. The saturation magnetic moment per V ion was determined to be $1.5\mu_B$ (Bohr magnetron) for x=0.13 V-doped $Sb_{2-x}V_xTe_3$ (shown in Fig. S6). This suggests that the valence state of V is a mixture of 3+ and 4+ (or/and 5+) as it is expected to substitute for the Sb^{3+} ion on the Sb sub-lattice.[17,18] The extra free electrons resulting from V^{4+} (or/and V^{5+}) go to neutralize the p-type carriers, so the n_{2D} of V-doped Sb_2Te_3 is expected and measured to be lower than that of Cr-doped samples, in which Cr takes the valence state 3+.[17,21]

The magnetic moment of V atom is smaller than that of Cr atom (~3μ_B),[17,21] and thus with exceptionally high H_c. The H_c in FM films, in addition to extrinsic influences such as defects that pin domain walls, depends on the magnetic anisotropy (both crystallographic and shape) and saturation magnetization moment (M_s) of the films. For magnetization reversal by the process of magnetic domain rotation, $H_c \propto \frac{K}{M_s}$, where K is the total magnetic anisotropy constant, so a higher K and/or lower M_s can lead to a high H_c. Since the demagnetization energy (E_d) determines the number of magnetic domain walls, and $E_d \propto {M_s}^2$, materials with few domains have a high H_c while those with many domains have a low H_c.[26,27] Therefore it is clear that V-doped Sb_2Te_3 with a lower M_s and a higher H_c have fewer magnetic domains than Cr-doped systems, indicating that the magnetic domains in V-doped Sb_2Te_3 are much larger in size than in Cr-doped films. The two main sources of magnetic anisotropy, magnetocrystalline anisotropy and surface anisotropy, appear to be very different for V- and Cr-doped Sb_2Te_3 films. The magnetocrystalline anisotropy is usually the most effective means of impeding the magnetization reversal by rotation processes, while the surface anisotropy is a major contributor in nm thick films. In high-quality epitaxial V-doped Sb_2Te_3 with large atomically flat areas, a near-perfect layered structure, and the slight expansion of c-axis lattice parameter may lead to the large magnetic anisotropy in the present films (see Supplementary Information).[26,27]

Due to the more robust ferromagnetism, V-doped Sb_2Te_3 films exhibit QAH state spontaneously without any magnetic field training, in sharp contrast to the Cr-doped systems.[14,15,16] Figure 3a shows the temperature-dependence of ρ_{xx} and ρ_{yx} for a different 4QL $(Bi_{0.29}Sb_{0.71})_{1.89}V_{0.11}Te_3$ film(sample S2), using a bottom gate bias V_g=0 and no applied magnetic field and cooled from room temperature under zero-field. ρ_{xx} shows semiconducting behaviors from room temperature down to ~2.5K, where a drop occurs, signaling that it is entering the

QAH state. ρ_{yx} remains constant from room temperature down to ~23K where it increases rapidly with further decreasing in temperature. This indicates that the system enters the FM state below ~23K. ρ_{yx} continues to increase and ρ_{xx} continues to decrease with decreasing temperature, ρ_{yx} approaches ~0.99h/e^2, and ρ_{xx} reaches ~0.30h/e^2 at the lowest temperature of the measurement at ~80mK. This behavior signifies the film spontaneously progressing toward the QAH state. The net magnetization of virgin state in the film, *i.e.* not induced by any external field, and the reduced thermal activation at lower temperature drives the film from the diffusive transport regime towards the conducting QAH state. The inset of Fig. 3a shows the low-temperature data at V_g=0V below 3K, for magnetic fields $\mu_0 H$=0 and 2T. This spontaneous decrease of ρ_{xx} at zero-field seen for V-doping is absent in Cr-doped TIs.[14,15,16] In Cr-doped TI films, unless the magnetic domains are aligned with an external applied perpendicular magnetic field, ρ_{xx} increases with decreasing temperature and no QAH state can be achieved even at very low temperatures.[15,16] Applying a field of 2T to the V-doped TI film, on the other hand, did not change the qualitative temperature dependence in ρ_{xx} and ρ_{yx}, from that of the zero-field cooling behavior. This clearly demonstrates that the macroscopic net magnetization of the virgin state in V-doped TIs is spontaneous and highly developed. The fact that virgin ρ_{yx} and ρ_{xx} curves overlap with the hysteresis loop (Fig. 3b) and the butterfly structure (Fig. 3c), also confirms the spontaneous self-magnetization of V-doped TI samples in the QAH regime. The high self-magnetization also appears in the direct magnetization measurements (see Supplementary Information).

The QAH state observed in V-doped TIs is unexpected from the view of first-principle calculations that points to the absence of an insulating FM state in V-doped TI due to the presence of *d*-orbital impurity bands in the bulk band gap.[12] Furthermore, in the QAH state

regime, the gate-voltage dependence of H_c of V-doped film (see Supplementary Information) is much larger than that of Cr-doped system,[14] also indicating the possible existence of FM induced from impurity bands, in addition to that from the van Vleck mechanism.[12]A possible explanation why there exists an insulating FM state could be that the *d*-orbital impurity bands become localized at lower temperatures, so that it does not participate in the charge transport and the whole system becomes an Anderson insulator instead of a band insulator. The localization physics in the QAH regime has been studied numerically in Ref. 10, which confirms that the QAH state can indeed be achieved in a metallic system by introducing disorder to localize bulk carriers. Thus, our experiments indicate the role of the localization physics of impurity bands in V-doped systems.

Our results demonstrate the high-precision confirmation of the QAH effect with the zero-field longitudinal resistance down to $0.00013\pm0.00007h/e^2$ (~$3.35\pm1.76\Omega$) and zero-field Hall conductance reaching up to ~$0.9998\pm0.0006e^2/h$ in V-doped $(Bi,Sb)_2Te_3$, a hard FMTI. It is particularly remarkable considering that mobility of the device measured near 80K is only ~$130cm^2/Vs$ (see Supplementary Information), orders of magnitude smaller than that found in semiconductor hetero-structures with two dimensional electron gas (2DEG) that reached the QH state.[1,2] This FMTI is found to be in the QAH state without the aid of a polarizing external magnetic field, making it a promising candidate for dissipationless electronic applications.

Methods

MBE growth. Thin film growth was performed using a custom-built ultrahigh vacuum MBE system. Semi-insulating etched Si(111), insulating heat-treated sapphire(0001) and $SrTiO_3(111)$ substrates were outgassed before the growth of TI films. High-purity Bi(99.999%), Sb(99.9999%), and Te(99.9999%) were evaporated from Knudsen effusion cells, whereas the transition metal dopants Cr(99.999%) and

V(99.995%) were evaporated by e-guns. During the growth, the substrate was maintained at 230℃. The flux ratio of Te per Bi and Sb was set to approximately ~8 to prevent Te deficiency in the films. The Sb, Bi, and V concentration in the films were determined by their ratio obtained in situ during growth using separate quartz crystal monitors and later confirmed ex situ by inductively coupled plasma atomic emission spectroscopy (ICP-AES). The growth rate for the films was approximately 0.2 quintuple layers per minute. Epitaxial growth was monitored by in situ reflection high energy electron diffraction (RHEED) patterns, where the high crystal quality and the atomically flat surface were confirmed by the streaky and sharp "1×1" patterns (see Supplementary Information).

Transport measurements. The transport measurements were performed ex situ on the magnetically-doped TI thin films. To avoid possible contamination, a 10-nm thick epitaxial Te capping layer was deposited at room temperature on top of the TI films before taken out of the growth chamber for transport measurements (see Supplementary Information). The Hall effect and longitudinal resistance were measured using both a Quantum Design Physical Property Measurement System (PPMS) (50mK, 9T) and a dilution refrigerator (Leiden Cryogenics, 10mK, 9T) with the excitation current flowing in the film plane and the magnetic field applied perpendicular to the plane. The bottom gate voltage was applied using the Keithley 6430. All the resistance meters were calibrated by a standard resistor. The QAH results reported here have been reproduced on several samples using the above two cryostats.

References

1. Klitzing, K. v., Dorda, G. & Pepper, M. New method for high-accuracy determination of the fine-structure constant based on quantized Hall resistance. *Phys. Rev. Lett.* **45**, 494-467 (1980).
2. Beenakker, C.W.J. and Houten, H. van. Quantum transport in semiconductor nanostructures. *Solid State Phys.* **44**, 1-228 (1991).
3. Haldane, F. D. M. Model for a quantum Hall effect without Landau levels: condensed-matter realization of the 'parity anomaly'. *Phys. Rev. Lett.* **61**, 2015-2018 (1988).

4. Onoda, M. and Nagaosa, N. Quantized anomalous Hall effect in two-dimensional ferromagnets: quantum Hall effect in metals. *Phys. Rev. Lett.* **90**, 206601 (2003).

5. Liu, C. X. *et al*. Quantum anomalous Hall effect in $Hg_{1-y}Mn_yTe$ quantum wells. *Phys. Rev. Lett.* **101**, 146802 (2008).

6. Qiao, Z. H. *et al*. Quantum anomalous Hall effect in graphene proximity coupled to an antiferromagnetic insulator. *Phys. Rev. Lett.* **112**, 116404 (2014).

7. Qiao, Z. H. *et al*. Quantum anomalous Hall effect in graphene from Rashba and exchange effects. *Phys. Rev. B* **82**, 161414(R) (2010).

8. Zhang, H. B. *et al*. Electrically tunable quantum anomalous Hall effect in graphene decorated by *5d* transition-metal adatoms. *Phys. Rev. Lett.* **108**, 056802 (2012).

9. Ezawa, M. Valley-polarized metals and quantum anomalous Hall effect in silicene. *Phys. Rev. Lett.* **109**, 055502 (2012).

10. Nomura, K. *et al*. Surface-quantized anomalous Hall current and the magnetoelectric effect in magnetically disordered topological insulators. *Phys. Rev. Lett.* **106**, 166802 (2011).

11. Garrity, K. F. and Vanderbilt, D. Chern Insulators from Heavy Atoms on Magnetic Substrates. *Phys. Rev. Lett.* **110**, 116802 (2013).

12. Yu, R. *et al*. Quantized anomalous Hall effect in magnetic topological insulators. *Science* **329**, 61-64 (2010).

13. Qi, X. L., Hughes, T. L. & Zhang, S. C. Topological field theory of time-reversal invariant insulators. *Phys. Rev. B* **78**, 195424 (2008).

14. Chang, C. Z. *et al*. Experimental observation of the quantum anomalous Hall effect in a magnetic topological insulator. *Science* **340**, 167-170 (2010).

15. Kou, X. *et al*. Scale-invariant dissipationless chiral transport in magnetic topological insulators beyond two-dimensional limit. *arXiv*:1406.0106 (2014).

16. Checkelsky, J. G. *et al*. T Trajectory of anomalous Hall effect toward the quantized state in a ferromagnetic topological insulator. *arXiv*:1406.7450 (2014).

17. Chien, Y. J. Transition metal-doped Sb_2Te_3 and Bi_2Te_3 Diluted Magnetic Semiconductors. Ph.D. Dissertation. The University of Michigan (2007).

18. Dyck, J. S. *et al*. Diluted magnetic semiconductors based on $Sb_{2-x}V_xTe_3$ ($0.01 \leq x \leq 0.03$). *Phys. Rev. B* **65**, 115212 (2002).

19. Hor, Y. S. *et al*. Development of ferromagnetism in the doped topological insulator $Bi_{2-x}Mn_xTe_3$. *Phys. Rev. B* **81**, 195203 (2010).

20. Zhang, J. *et al*. Band structure engineering in $(Bi_{1-x}Sb_x)_2Te_3$ ternary topological insulators. *Nat. Commun.* **2**, 574 (2011).

21. Chang, C. Z. *et al*. Thin films of magnetically doped topological insulator with carrier-independent long-range ferromagnetic order. *Adv. Mater.* **25**, 1065-1070 (2013).

22. ρ_{yx} and ρ_{xx} results shown in Fig. 1 were carried out with excitation current of 1 nA and with the mixing chamber of the dilution refrigerator anchored at 10 mK. However, systematic measurements of ρ_{xx} as functions of temperature and (higher) excitation current indicate the electron temperature of the sample is ~25±5mK due to the stray electromagnetic noise.

23. Arrott, A. Criterion for Ferromagnetism from Observations of Magnetic Isotherms. *Phys. Rev. B* **108**, 1394 (1957).

24. He, K. *et al*. Quantum anomalous Hall effect. *Natl. Sci. Rev.***1**, 39-49 (2014).

25. Nagaosa, N. *et al.* Anomalous Hall effect. *Rev. Mod. Phys.* **82**, 1539-1592 (2010).

26. Coey, J. M. D. Magnetism and magnetic materials. Cambridge University Press, New York (2009).

27. Livingston, J. D. A review of coercivity mechanisms. *J. Appl. Phys.* **52(3)**, 2544-2548 (1981).

Acknowledgements

We are grateful to P. Wei, J. Liu, J. Wang, L. Fu, N. Samarth, J. Jain and G. Csathy and Z. Fang for helpful discussions, and F. Katmis, W. J. Fang, C. Settens and J. Kong for technical support in characterizing the samples. This research is supported by the grants NSF (DMR-1207469), NSF (DMR-0907007), ONR (N00014-13-1-0301), NSF (DMR-0820404, Penn State MRSEC), NSF (DMR-1103159),

DOE (DE-AC02-76SF00515), DARPA (N66001-11-1-4105) and the STC Center for Integrated Quantum Materials under NSF grant DMR-1231319.

Author contributions

C. Z. C., M. H. W. C. and J. S. M. conceived and designed the research. C. Z. C. grew the material with the help of J. S. M.. C. Z. C. performed characterization studies of the samples with the help of B. A. A. and D. H.. W. Z. made the devices and performed the transport measurements with the help of C. Z. C., D. K. and M. H. W. C.. C. X. L., H. J. Z. and S. C. Z. provided theory support. C. Z. C., C. X. L., and M. H. W. C. analyzed the data and wrote the manuscript with contributions from all authors.

Additional information

Supplementary information is available in the online version of the paper. Reprients and permissions information is available at www.nature.com/reprints.

Correspondences and requests for materials should be addressed to C. Z. C., W. Z. or J. S. M..

Competing financial interests

The authors declare no competing financial interests.

Figures and Figure captions:

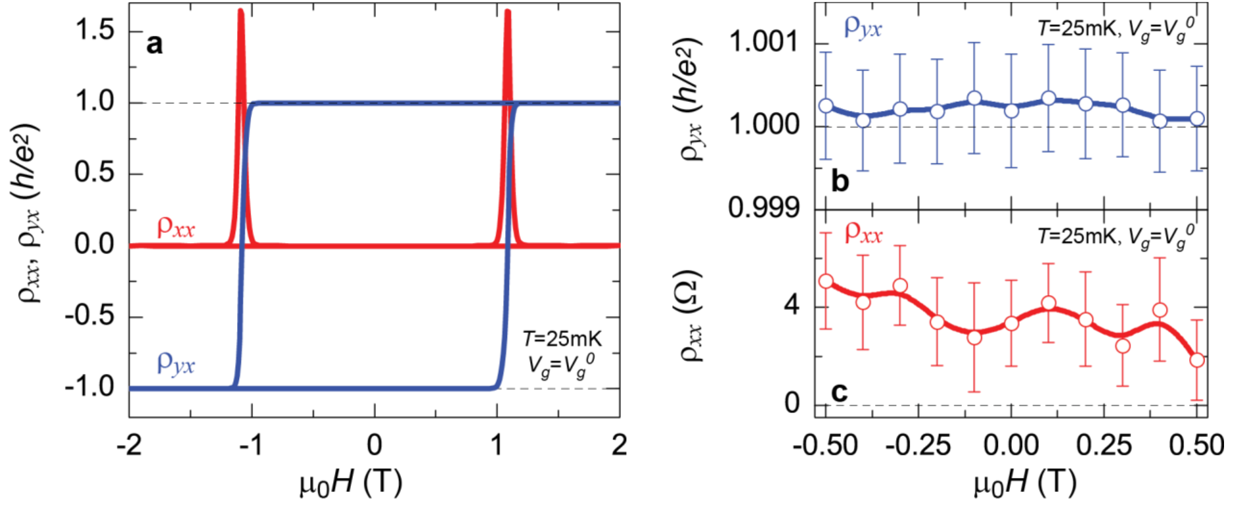

Figure 1 | The QAH effect in a 4QL $(Bi_{0.29}Sb_{0.71})_{1.89}V_{0.11}Te_3$ film (sample S1) measured at 25mK. a, Magnetic field dependence of the longitudinal resistance ρ_{xx} (red curve) and the Hall resistance ρ_{yx} (blue curve) at charge neutral point $V_g=V_g^0$. **b**, **c**, Expanded ρ_{yx} (**b**) and ρ_{xx} (**c**) at low magnetic field. ρ_{yx} at zero magnetic field exhibits a value of $1.00019\pm0.00069h/e^2$, while ρ_{xx} at zero magnetic field is only $\sim0.00013\pm0.00007h/e^2$ ($\sim3.35\pm1.76\Omega$).

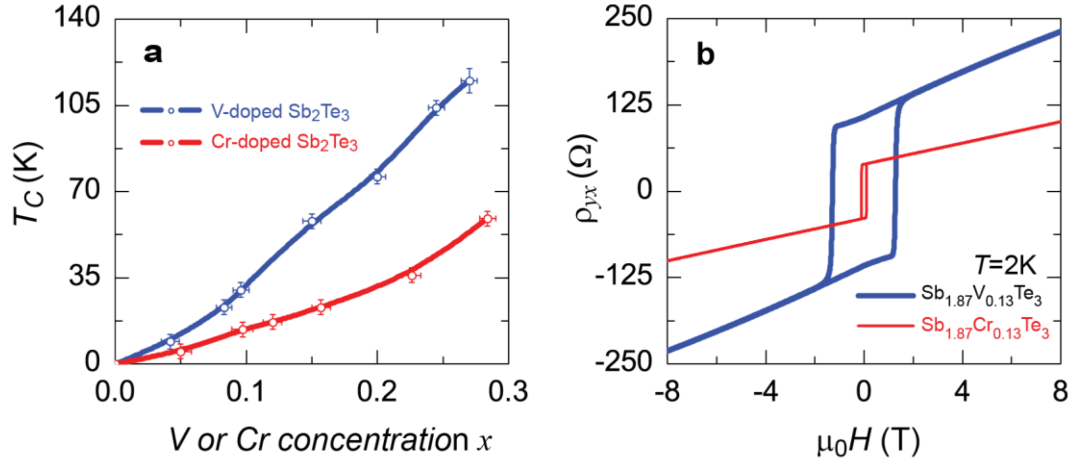

Figure 2 | Ferromagnetic properties comparing Cr- and V-doped Sb_2Te_3. a, The Curie temperature (T_C) of 6QL $Sb_{2-x}V_xTe_3$ (blue circles) and $Sb_{2-x}Cr_xTe_3$ thin films (red circles). Note the factor of 2 increase in T_C for V doping. **b**, The Hall traces of 6QL $Sb_{1.87}V_{0.13}Te_3$ and $Sb_{1.87}Cr_{0.13}Te_3$ thin films, measured at T=2K. Note the order of magnitude increase in H_c for V doping.

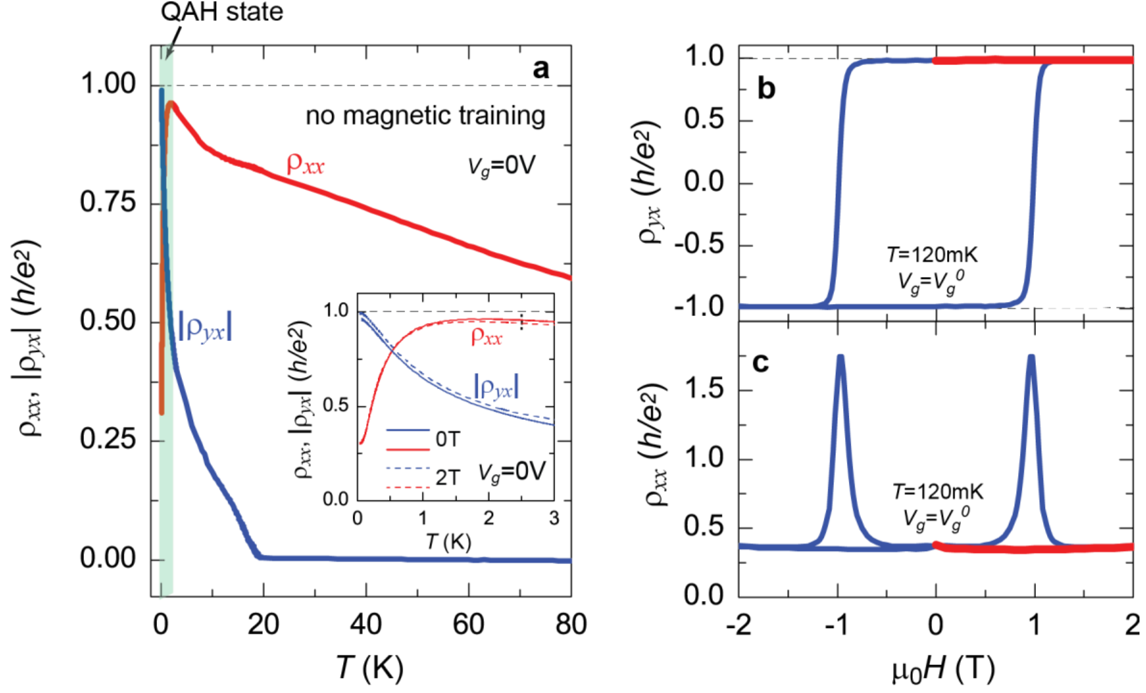

Figure 3 | The self-driven QAH state in a different 4QL $(Bi_{0.29}Sb_{0.71})_{1.89}V_{0.11}Te_3$ film (sample S2). a, Temperature dependence of longitudinal resistance ρ_{xx} (red curve) and Hall resistance $|\rho_{yx}|$ (blue curve) of sample S2 without magnetic training. Inset: T-dependent ρ_{xx} (red curve) and $|\rho_{yx}|$ (blue curve) under magnetic field μ_0H=0 (solid) and 2T (dashed). The opposite T-dependent behaviors of ρ_{xx} and $/\rho_{yx}/$ reveal the QAH state at low T. **b, c**, The magnetic field-dependent ρ_{yx} (**b**) and ρ_{xx} (**c**) of sample S2 measured at 120mK. The red curves in **b** and **c** were obtained by first cooling the sample under zero-field and then measured from zero to higher field.